JACS
JOURNAL OF THE AMERICAN CHEMICAL SOCIETY
Article
Cite This: J. Am. Chem. Soc. 2019, 141, 972−980
pubs.acs.org/JACS

Mechanistic Study of Ruthenium-Catalyzed C−H Hydroxylation Reveals an Unexpected Pathway for Catalyst Arrest

James B. C. Mack,[‡] Katherine L. Walker,[‡] Sophia G. Robinson,[§] Richard N. Zare,*[,‡] Matthew S. Sigman,*[,§] Robert M. Waymouth,*[,‡] and J. Du Bois*[,‡]

[‡]Department of Chemistry, Stanford University, 337 Campus Drive, Stanford, California 94305, United States
[§]Department of Chemistry, University of Utah, 315 South 1400 East, Salt Lake City, Utah 84112, United States

Supporting Information

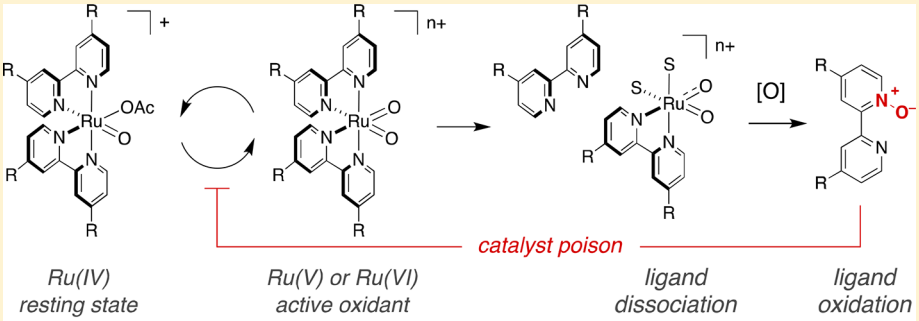

ABSTRACT: We have recently disclosed [$(dtbpy)_2RuCl_2$] as an effective precatalyst for chemoselective C−H hydroxylation of $C(sp^3)$−H bonds and have noted a marked disparity in reaction performance between 4,4′-di-*tert*-butyl-2,2′-bipyridine (dtbpy)- and 2,2′-bipyridine (bpy)-derived complexes. A desire to understand the origin of this difference and to further advance this catalytic method has motivated the comprehensive mechanistic investigation described herein. Details of this reaction have been unveiled through evaluation of ligand structure−activity relationships, electrochemical and kinetic studies, and pressurized sample infusion high-resolution mass spectrometry (PSI-MS). Salient findings from this investigation include the identification of more than one active oxidant and three disparate mechanisms for catalyst decomposition/arrest. Catalyst efficiency, as measured by turnover number, has a strong inverse correlation with the rate and extent of ligand dissociation, which is dependent on the identity of bipyridyl 4,4′-substituent groups. Dissociated bipyridyl ligand is oxidized to mono- and bis-*N*-oxide species under the reaction conditions, the former of which is found to act as a potent catalyst poison, yielding a catalytically inactive tris-ligated $[Ru(dtbpy)_2(dtbpy\ N\text{-oxide})]^{2+}$ complex. Insights gained through this work highlight the power of PSI-MS for studies of complex reaction processes and are guiding ongoing efforts to develop high-performance, next-generation catalyst systems for C−H hydroxylation.

INTRODUCTION

The evolution of catalytic methods for selective C−H bond oxidation has transformed the practice of complex molecule synthesis.[1] These technologies provide single-step access to value-added products, including modified natural products, active pharmaceutical ingredients, and drug metabolites.[2] The prevalence of reports describing new catalysts and protocols for C−H oxidation notwithstanding, efficient chemo- and site-selective functionalization of substrates bearing polar functional groups, and in particular nitrogen-based substituents, remains a formidable challenge for methods development.[3,4] Recent disclosures from our lab and others capitalize on seminal work by Adam and co-workers to address the intrinsic problems with oxidative cross-reactivity of amines and azaheterocycles.[5,6] To this end, we have demonstrated that a mononuclear Ru-catalyst derived from 4,4′-di-*tert*-butyl-2,2′-bipyridine (dtbpy), *cis*-$[Ru(dtbpy)_2X_2]$, functions as an efficient precatalyst for oxidation of 3° and benzylic C−H bonds in aqueous acid medium.[7] Efforts to improve the scope and performance of this chemistry have motivated mechanistic studies to understand off-pathway reactions that limit catalyst turnover numbers. These investigations have revealed an unexpected pathway for catalyst arrest that illuminates the link between ligand substitution and catalyst performance.

BACKGROUND

Prior work from our laboratories has shown that both $[Ru(Me_3tacn)Cl_3]$ (Me_3tacn = *N*,*N*′,*N*″-trimethyl(1,4,7-triazacyclononane)) and *cis*-$[Ru(dtbpy)_2Cl_2]$ function as effective precatalysts for C−H oxidation using terminal oxidants such as ceric ammonium nitrate (CAN), $NaIO_4$, and H_5IO_6.[4a,8,9] A

Received: October 10, 2018
Published: January 2, 2019

Downloaded via STANFORD UNIV on January 18, 2019 at 18:22:19 (UTC).
See https://pubs.acs.org/sharingguidelines for options on how to legitimately share published articles.

© 2019 American Chemical Society

DOI: 10.1021/jacs.8b10950
J. Am. Chem. Soc. 2019, 141, 972−980

salient feature of these catalyst systems is kinetic stability in aqueous acid. By comparison, first-row catalysts are generally unstable under oxidizing conditions in aqueous solution.[10] The use of aqueous acid as a solvent medium solubilizes polar substrates and retards amine reactivity through protonation.

Although [Ru(Me$_3$tacn)Cl$_3$] affords turnover numbers (TONs; TON = mol product/mol Ru) of 5−80 with select substrates, catalyst modification to improve scope and efficiency is severely restricted by an inflexible ligand design. In contrast, substituted 2,2′-bipyridines can be used to generate an array of sterically and electronically disparate *cis*-(bpy)$_2$Ru(II)X$_2$ complexes that serve as precatalysts for C−H oxidation (Figure 1). For the purpose of exploring catalyst structure−function, this system is considerably advantaged over Ru-tacn.

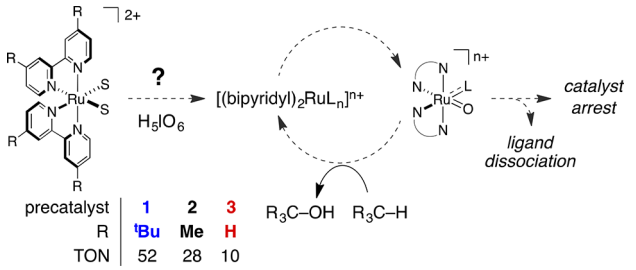

Figure 1. Mechanistic study of Ru-catalyzed C−H hydroxylation reaction to understand differences in precatalyst performance. Turnover numbers (TONs) determined from reactions performed with 0.5 mol % catalyst loading.

We have employed a suite of electrochemical, spectroscopic, and modern spectrometric analysis methods to interrogate the mechanism of Ru-catalyzed C−H oxidation. These studies have been guided by three overarching questions: (1) what is the influence of bipyridine structure on catalyst TONs; (2) what is the nature of the active Ru-oxidant(s); (3) what is (are) the pathway(s) for inhibition of reaction turnover and/or catalyst arrest. Our work has culminated in the surprising discovery of a mechanism for catalyst arrest involving ligand dissociation and oxidation to form a catalyst poison. Insights afforded from these findings will guide the design of high-performance, next-generation C−H oxidation catalysts.

RESULTS AND DISCUSSION

Precatalyst SAR and Reaction TON. To better understand the effects of catalyst structure on TON, we examined [bis(bipyridyl)RuX$_2$] catalysts bearing differentially substituted bipyridine ligands.[11] Attempted preparation of these complexes using a reported literature route (2 equiv of ligand, RuCl$_3$, refluxing dimethylformamide (DMF)) generally yielded mixtures of mono-, bis-, and tris-ligated Ru(II) and Ru(III) complexes.[12] Changing solvent and Ru salt afforded significantly improved product yields and a reliable method for preparing new [bis(bipyridyl)RuCl$_2$] precatalysts (Scheme 1, method A).[13] With select ligands, however, isolation of pure product remained difficult. The addition of carbonate offered a convenient solution to the separations problem, allowing for isolation of a single Ru species as the carbonate adduct (Scheme 1, method B). The chelating nature of the carbonate ligand presumably biases formation of the *cis*-configured [bis(bipyridine)Ru(CO$_3$)] complex. This protocol may prove effective for generating other *cis*-configured Ru derivatives.

Scheme 1. Synthesis of Dichloro- and η^3-Carbonato-Ru(II) Precatalysts

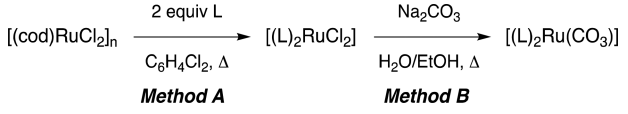

A series of Ru-precatalysts derived from chelating dipyridyl ligands was evaluated under a standard protocol in an oxidation reaction of 3-methylpentyl benzoate **5** (5 mol % catalyst, H$_5$IO$_6$ or (NH$_4$)$_2$Ce(NO$_3$)$_6$, AcOH/H$_2$O, 4 h, Table 1). Notably, dichloro- and carbonato-derived complexes performed equivalently in all cases examined (entries 1 and 2, 4 and 5). In general, precatalysts derived from electron-rich bipyridine ligands (e.g., alkyl-, MeO-) displayed the highest TONs (entries 1−3, 6, and 7).[14] Among the precatalysts tested, *cis*-[Ru(dtbpy)$_2$(CO$_3$)] (**1**), was distinguished as the top performer (entry 1), matched only by *cis*-[Ru(4,4′-(MeO)$_2$-bpy)$_2$(CO$_3$)] (**4**) in combination with a large excess of (NH$_4$)$_2$Ce(NO$_3$)$_6$ (entry 7).

Table 1. Examination of Ru Precatalysts for C−H Hydroxylation[a]

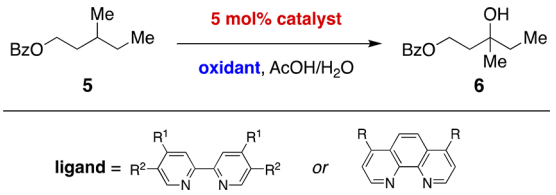

entry	ligand	counterion	oxidant (equiv)	% 6	TON
1[b]	R^1 = ^{t}Bu	CO_3	H_5IO_6 (2)	58	11.6
2[b]	R^1 = ^{t}Bu	2 Cl	H_5IO_6 (2)	58	11.6
3[b]	R^1 = Me	CO_3	H_5IO_6 (2)	40	8.0
4[b]	R^1 = H	CO_3	H_5IO_6 (2)	22	4.4
5[b]	R^1 = H	2 Cl	H_5IO_6 (2)	22	4.4
6[b]	R^1 = OMe	CO_3	H_5IO_6 (2)	34	6.8
7[b]	R^1 = OMe	CO_3	CAN (6)	61	12.2
8[c]	R^1 = Me, R^2 = F	2 Cl	CAN (3)	28	5.6
9[b]	R^1 = Ph	2 Cl	H_5IO_6 (2)	6	1.2
10[b,c]	R^1 = Mes	2 Cl	CAN (3)	trace	<1
11[b]	R^1 = Br	2 Cl	H_5IO_6 (2)	trace	<1
12	R = H	2 Cl	H_5IO_6 (2)	8	1.6
13	R = Me	2 Cl	H_5IO_6 (2)	18	3.6

[a]Reactions were conducted on 0.10 mmol scale. Conditions: 5 mol % *cis*-[(ligand)$_2$RuCl$_2$] or *cis*-[(ligand)$_2$Ru(CO$_3$)] (3.125 mM), 2.0−6.0 equiv of oxidant (125−375 mM), AcOH/H$_2$O, 4 h. Product conversions estimated by ^{1}H NMR integration of unpurified reaction mixtures against an internal standard. [b]R^2 = H. [c]Oxidation of **5** is not productive with H$_5$IO$_6$; CAN = (NH$_4$)$_2$Ce(NO$_3$)$_6$.

To gain additional insight into the link between ligand structure and catalyst TON, reaction progress was monitored by ^{1}H NMR (Figure 2). For this analysis, oxidation of substrate **5** was analyzed using precatalysts *cis*-[Ru(dtbpy)$_2$(CO$_3$)] (**1**), *cis*-[Ru(dmbpy)$_2$(CO$_3$)] (**2**) (dmbpy = 4,4′-dimethyl-2,2′-bipyridine), and *cis*-[Ru(bpy)$_2$(CO$_3$)] (**3**). The efficiencies of these three complexes for C−H hydroxylation are varied despite modest differences in structure (see Figure 1).[15] All three precatalysts show an

DOI: 10.1021/jacs.8b10950
J. Am. Chem. Soc. 2019, 141, 972−980

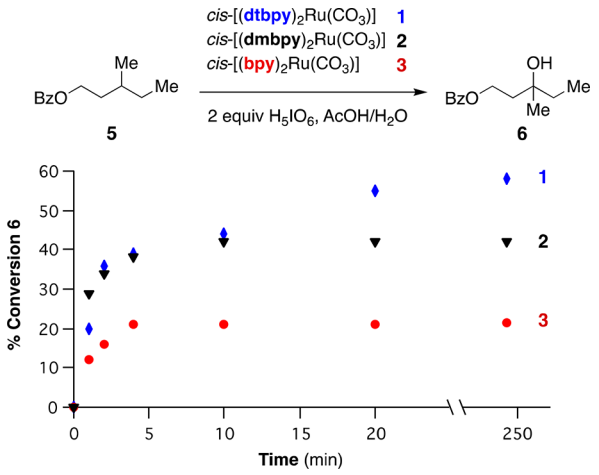

Figure 2. Reaction progress kinetic profiles of precatalysts **1**, **2**, and **3** in the oxidation of **5**. Conditions: 5 mol % *cis*-[(ligand)$_2$Ru(CO$_3$)] (3.125 mM), 2.0 equiv of H_5IO_6 (125.0 mM), AcOH/H_2O. Product conversions estimated by ^{1}H NMR integration of unpurified reaction mixtures against an internal standard.

initial phase of rapid product formation during the first 5 min of reaction (Figure 2). Complexes **1** and **2** feature a second phase of product formation before plateauing at 10 and 20 min, respectively. By contrast, the reaction with **3** reaches completion within ∼4 min. From these data, it appears that reaction performance is correlated with catalyst lifetime and not intrinsic differences in catalyst activity. Accordingly, subsequent experiments were devised to challenge this conclusion.

Electrochemical Studies of Precatalysts 1−4. Electrochemical measurements were conducted with precatalysts **1**−**4** to compare the redox potentials of the different Ru species and to determine if more than one Ru oxidant was capable of hydroxylating substrate. Cyclic vol (CVs) tammograms of each precatalyst were recorded in aqueous $HClO_4$ and in AcOH/aqueous $HClO_4$ mixtures in the absence and presence of substrate (Figures 3, S2 and S3).[16] Meyer previously reported

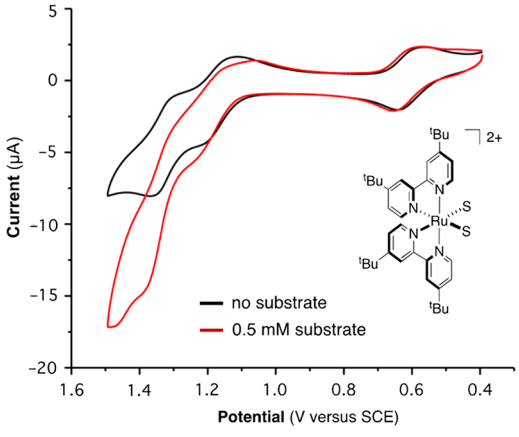

Figure 3. Cyclic voltammograms of 1 mM *cis*-[(dtbpy)$_2$Ru(CO$_3$)] **1** in 1:1 AcOH/0.75 M aqueous $HClO_4$; (pH 0.5) in the absence and presence of substrate. Cyclic voltammetry performed with a 10 mV/s scan rate using a glassy carbon working electrode, platinum mesh counter electrode, and SCE reference electrode. The substrate for these experiments is 2-amino-6-methylheptane; see Supporting Information for details.

that *cis*-[(bpy)$_2$Ru(CO$_3$)] (**3**) in aqueous $HClO_4$ cycles reversibly between five oxidation states, Ru(II) to Ru(VI).[17] Related studies characterized [(6,6′-Cl$_2$bpy)$_2$Ru(O)$_2$]$^{2+}$, a *cis*-configured Ru(VI)-dioxo adduct, and demonstrated that this complex can promote stoichiometric C−H hydroxylation of simple alkanes.[18] Substrate oxidation by a Ru(V)-oxo or -dioxo intermediate also appears to be possible based on the available electrochemical data.

Cycling of **1** from 0.4 to 1.5 V at a 10 mV/s scan rate afforded a fully reversible redox wave (black trace) that reflects multiple Ru oxidation states and is analogous to data recorded by Meyer with **3**.[19] Redox waves at 0.6, 1.2, and 1.35 V (vs SCE) were thus assigned as Ru(II)/Ru(III), Ru(IV)/Ru(V), and Ru(V)/Ru(VI) couples, respectively. To determine which form(s) of **1** might participate in C−H hydroxylation, cyclic voltammograms were obtained with added substrate (0.5 mM, Figure 3, red trace).[20] In these experiments, a small current increase was noted at 1.20 V with a second, more substantial rise in current as the potential was scanned past 1.30 V. The increase in current at a given potential is indicative of electrocatalytic oxidation.[20] Conversely, the absence of a change in current below ∼1.18 V implies that Ru oxidation states of **1** below this applied potential are unreactive with substrate. This conclusion is supported by a series of constant potential bulk electrolysis reactions in which no substrate oxidation was detected at potentials below 1.15 V (Table S3).

Data obtained from CV and bulk electrolysis experiments with precatalyst **1** in the presence of substrate are consistent with an electrocatalytic process mediated by a Ru(VI) oxidant. The structure of this intermediate is presumed to be *cis*-[(dtbpy)$_2$Ru(O)$_2$]$^{2+}$ by inference to prior work.[17] The small increase in current at 1.2 V (red trace, Figure 3) suggests, but does not conclusively establish, that a Ru(V) species may also function as a competent oxidant. The closeness of the onset potentials for Ru(V) and Ru(VI) further obscures this analysis. Analogous experiments with precatalysts **2**−**4** led to the same conclusions, as peak potentials for Ru(IV)/Ru(V) and Ru(V)/Ru(VI) couples are within error for all four complexes examined (Figure S1).

CV recordings show no evident link between catalyst structure, thermodynamic redox potential, and reaction performance. In addition, these experiments fail to provide definitive evidence for Ru(V) as an active oxidant, although the reactivity of Ru(VI) with substrate is clear.[21] Accordingly, with the goal of understanding performance differences between precatalysts **1**−**3** (see Figure 1), experiments using alternative analytical methods, including NMR and mass spectrometry, were pursued.

^{19}F NMR Spectroscopy and Mass Spectrometric Investigations of Catalyst Speciation. ^{19}F NMR spectroscopy provides a useful analytical method for tracking catalyst speciation as a function of reaction progress.[22] In order to measure catalyst lifetime and to gain insight into the distribution of Ru products formed throughout the course of the hydroxylation reaction, a Ru(II) precatalyst derived from 5,5′-difluoro-4,4′-dimethyl-2,2′-bipyridine (**7**) was prepared (Figure 4). Analysis of the spent oxidation reaction of **5** with precatalyst **7** performed under standard conditions revealed the primary ^{19}F-signal to be that of free ligand. This result is consistent with early work of Meyer and gives the first clue that ligand dissociation may be a primary degradation event limiting catalyst TONs.[17]

DOI: 10.1021/jacs.8b10950
J. Am. Chem. Soc. 2019, 141, 972−980

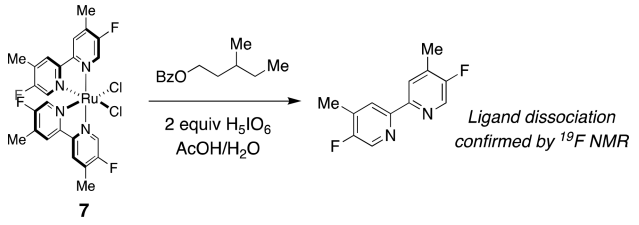

Figure 4. ^{19}F NMR spectroscopy reveals loss of ligand in the oxidation of **5** by fluorine-substituted catalyst **7**; see Supporting Information for experimental details.

Subsequent experiments aimed at tracking reaction progress through ^{19}F NMR spectroscopy were attempted, but were unable to provide useful information regarding catalyst speciation. These studies were confounded by the poor signal-to-noise of the ^{19}F spectra, in part due to the paramagnetism of some of the Ru intermediates. Reaction monitoring by real-time mass spectrometry thus became the method of choice for analyzing catalyst speciation and decomposition pathways.

Mass spectrometry is ideally suited for studying catalyst speciation in our C−H oxidation reaction given the unique isotopic fingerprint of Ru. In practice, *in situ* monitoring of the Ru-catalyzed reaction is possible using pressurized sample infusion mass spectrometry (PSI-MS).[23] This method enables continuous infusion of a sample from a reaction that is performed in a conventional round-bottom flask setup under standard conditions. Temporal resolution of ion counts permits correlation of different analytes with kinetic events relevant to reaction catalysis.[24] Accordingly, we anticipated that data obtained from PSI-MS could provide key insights into the reaction mechanism and catalyst degradation pathways.

For the PSI-MS study that follows, speciation of precatalyst **1** was examined for reactions with H_5IO_6 in the absence and presence of substrate **5** (Figures 5 and S5−S11). The carbonato form of **1** was selected for this analysis, as the dichloro derivative produced more complex (due to splitting from multiple chloride isotopes) and often overlapping signals in the mass chromatogram, thus complicating analysis.[25] Additional Ru-containing ions that are not highlighted in the following discussion are, in large part, related analytes with additional MeCN ligands or different counterions or charges (details can be found in the Supporting Information). Putative structures of individual ions are inferred using tandem MS/MS methods and, when possible, by direct comparison of MS data with authentic samples.

Initial PSI-MS control experiments were performed in the absence of substrate with precatalyst **1** (3.125 mM) and H_5IO_6 (125.0 mM) (Figure S11). Upon addition of H_5IO_6, two prominent ions centered at m/z 713.3004 and 845.1694 are immediately detected. Within 3 min of initiating the reaction, both of these species are no longer present (Figure S11).[26] These signals correspond to a Ru(IV)-oxo and a Ru(VI)-dioxo species, respectively, with assignments supported by collision-induced dissociation (CID) MS/MS data (structures appear in Figure 5B). Prior work by Meyer has indicated that the Ru(VI)-dioxo form of precatalyst **3**, $[(bpy)_2Ru(O)_2]^{2+}$, is quite labile and degrades within seconds following generation.[17] Therefore, it is notable that PSI-MS enables detection of the analogous complex generated from **1**.

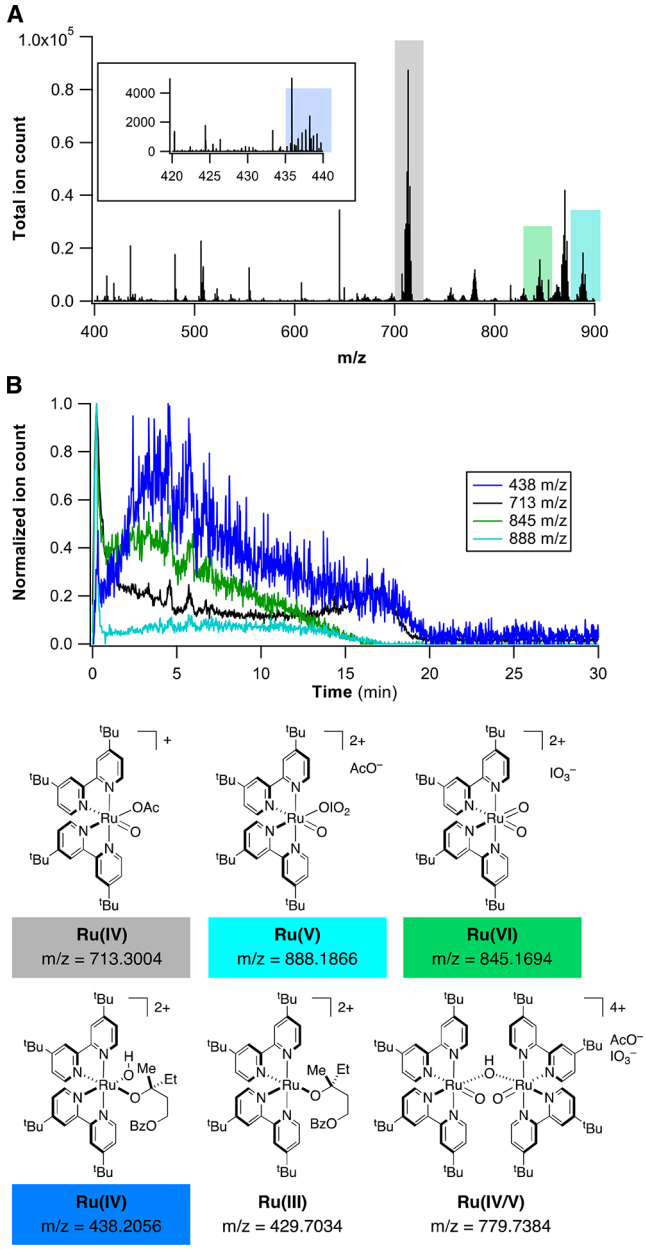

Figure 5. (A) Mass chromatogram from m/z 400 to 900 taken at 0.5 min of a reaction containing 5 mol % **1**, 1.0 equiv of **5**, and 2.0 equiv of H_5IO_6. Inset: Spectrum from m/z 420 to 440. (B) Extracted ion chromatographs of select Ru species. Each trace is normalized to the total ion count, and the highest intensity is set to 1.0. Dead time offset of −0.5 min has been applied.

Performing the equivalent PSI-MS experiments in the presence of substrate **5** (62.5 mM) shows the same ions at 713.3004 and 845.1694, along with a third prominent ion at m/z 888.1866 (Figure 5). We have assigned this latter species as a Ru(V)-oxo complex. All three high-valent intermediates appear rapidly upon addition of H_5IO_6; however, with substrate present, the ion counts corresponding to these analytes do not deplete until 15−20 min (Figure 5B, black, teal, green traces). As the cyclic voltammetry and bulk electrolysis data indicate that Ru species formed at potentials below ~1.18 V are unreactive toward substrate (*vide supra*), we surmise that the Ru(IV) ion at m/z 713.3004 is a resting state of the catalyst, not responsible for direct turnover of product.

DOI: 10.1021/jacs.8b10950
J. Am. Chem. Soc. 2019, 141, 972−980

Among the different Ru analytes formed in reactions with substrate **5**, including the aforementioned high-valent Ru-oxo and -dioxo ions, two species at m/z 438.2056 and 429.7034 are particularly telling of the reaction mechanism (Figure 5B). These intermediates have been assigned as substrate-bound ruthenium complexes (i.e., Ru-alkoxides). The identification of $[(dtbpy)_2Ru(OH)(OR)]^{2+}$ at m/z 438.2506 provides strong evidence for the role of a Ru(VI)-dioxo oxidant as an active hydroxylating agent under the reaction conditions. Formation of this product could occur through either a canonical C−H abstraction/radical rebound mechanism or a concerted [3 + 2] cycloaddition, both of which have been proposed for *cis*-dioxo-Ru C−H hydroxylation reactions.[27,28] Similarly, the ion at m/z 429.7034 corresponding to the Ru(III)-alkoxide could plausibly derive from substrate reacting with a Ru(V)-oxo species.

Having obtained support from complementary electrochemical and MS experiments for the generation of, at minimum, two active oxidants, we next attempted to determine the reaction mechanisms and structures of catalyst products responsible for inhibiting turnover. Among the different pathways that may result in catalyst degradation or arrest, we initially considered two: dimerization (pathway 1, Figure 6)

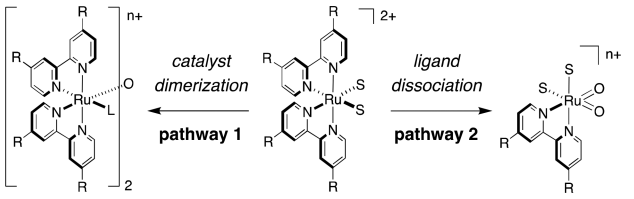

Figure 6. Postulated degradation mechanisms of [bis(bipyridyl)-RuX_2] precatalysts under oxidative conditions. R = H, Me, or ^{t}Bu.

and ligand dissociation (pathway 2).[29] In the latter case, the resulting monoligated (bpy)Ru complex is unlikely to support catalysis.[30] Our analysis of these processes capitalized on the availability of three structurally related precatalysts, **1**−**3**, and the evident differences in reaction performance between these complexes (see Figure 1).

PSI-MS Study of Catalyst Dimerization. Catalyst dimerization (pathway 1, Figure 6) is commonly invoked with reactive metal-oxo species and was assumed a likely pathway for catalyst inactivation.[31] When precatalyst **1** is mixed with H_5IO_6 and substrate **5**, PSI-MS reveals an ion at m/z 779.7384 that corresponds to a dimeric Ru(IV/V) species. This signal appears within 1 min and then dissipates over the course of 20 min (see Figures 5, S8). The transient nature of this ion suggests that this particular species is kinetically labile under the reaction conditions. Interestingly and in spite of the excess of H_5IO_6 used in this process, lower valent dimeric complexes (e.g., Ru(III/IV), Ru(IV/IV)) are detected within ∼10 min of initiating the reaction (Figure 7); signals ascribed to these species increase until the reaction no longer proceeds. The ion count for these two complexes is quite low, and, thus, we posit that dimer formation is only partly responsible for catalyst arrest. Dimeric adducts of precatalysts **2** and **3** are not detected at all when monitored by PSI-MS. Collectively, these results are rather surprising given the predilection for reactive metal-oxo species to aggregate.[31] In our prior studies with $[Ru(Me_3tacn)Cl_3]$, dimerization was identified as the primary mode of catalyst inactivation.[31d] As dimer formation is unable to fully account for differences in catalyst performance,

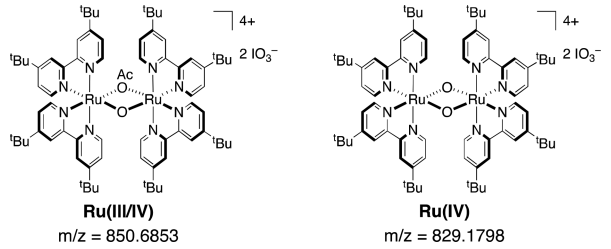

Figure 7. Proposed structures of stable Ru dimers.

mechanisms involving ligand dissociation were subsequently interrogated.

PSI-MS and HPLC Evaluation of Ligand Dissociation. In accordance with data from ^{19}F NMR studies (*vide supra*), PSI-MS confirms that ligand dissociation occurs for all three precatalysts examined (Figure S46−S49). Mono- and bis-*N*-oxidized ligand products are detected in addition to free ligand. These data give qualitative evidence for marked differences in the rate of ligand dissociation between the three precatalysts. Signals correlating with monobipyridyl-Ru adducts appear at early reaction time points for precatalysts **2** and **3**, but not for **1** (Figures S35, S39).[32] Additionally, for complexes **2** and **3**, detection of free ligand and product formation appear to reach a maximum at the same time point; this is not the case for precatalyst **1**. These findings strongly implicate ligand dissociation as a deleterious process that limits reaction turnover. The heightened performance of **1** appears to derive from the kinetic stability of the oxidized form(s) of the $(dtbpy)_2Ru$ complex with respect to ligand exchange.

In support of the results from our PSI-MS study, we have quantified by HPLC ligand dissociation as a function of reaction progress (Figure 8). A standard oxidation reaction was performed and sampled at different time points to measure free ligand concentration in addition to mono- and bis-*N*-oxide products, which were also detected. Consistent with our MS data, the total amount of dissociated ligand is lowest (∼20%) in experiments with precatalyst **1**. By comparison, complex **3**

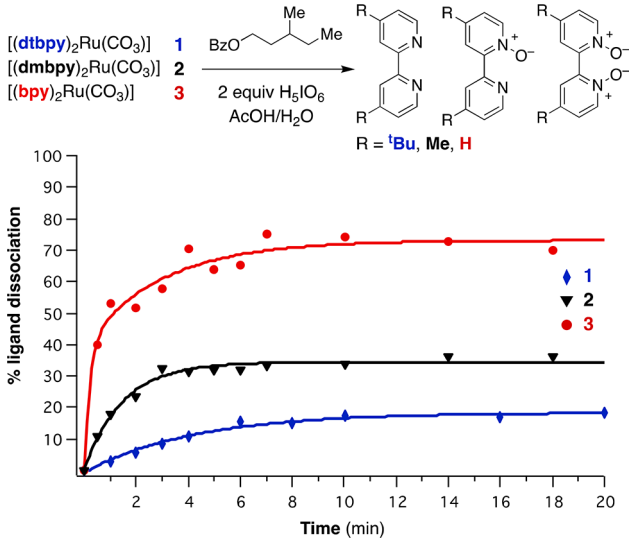

Figure 8. Quantitative HPLC evaluation of ligand loss versus time for catalysts **1**−**3** in the oxidation of substrate **5**. Percentage of total ligand dissociation assumes 1 equiv per catalyst; see Supporting Information for details.

DOI: 10.1021/jacs.8b10950
J. Am. Chem. Soc. 2019, 141, 972−980

rapidly loses a bpy group, reaching a maximum (>70%) within minutes after the reaction commences. Peak ligand loss is coincident with cessation of catalyst turnover. Thus, the major pathway that limits TONs with precatalyst **3** is ascribed to ligand dissociation (pathway 2, Figure 6). Conversely, the absence of such a correlation with precatalyst **1** intimates that more than one pathway leading to catalyst decomposition/inactivation is operative.

Identification of a Catalyst Arrest Mechanism. PSI-MS data for reactions with **1** were further examined to understand the differential performance of this precatalyst. From this analysis, a prominent signal at m/z 461.2406 was identified as a tris(bipyridyl)Ru(II) complex (**8**) (Figure 9). The structure of

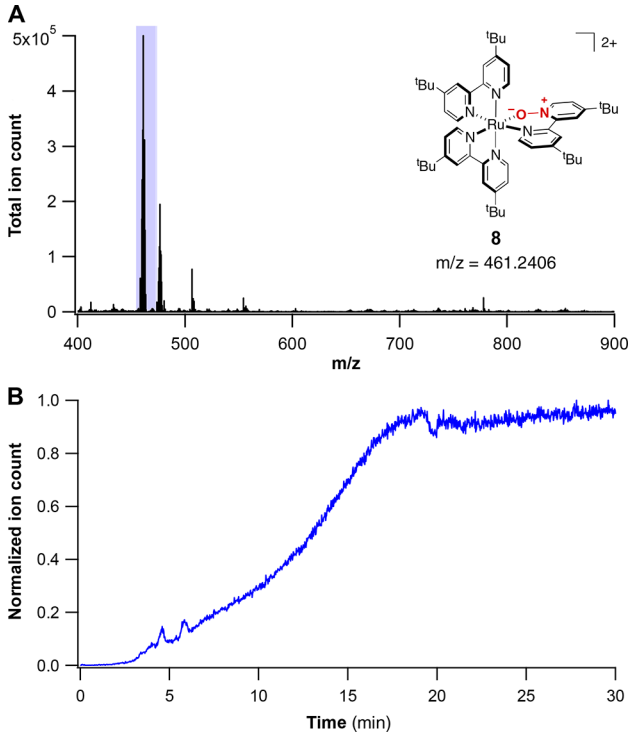

Figure 9. (A) Mass spectrum from m/z 400 to 900 obtained from a reaction with precatalyst **1** at 23 min. (B) Extracted ion chromatograph of tris-bipyridyl Ru complex **8** recorded over the reaction time course. The trace is normalized to the total ion count, and the highest intensity is set to 1. A dead time offset of −0.5 min has been applied.

adduct **8** was suggested from MS and MS/MS analysis to comprise two dtbpy ligands and one dtbpy *N*-oxide.[33] Interestingly, maximum ion counts for **8** coincide with the time the reaction catalyzed by **1** takes to reach completion (~20 min).[34,35]

Detection of the tris-complex **8** is quite surprising in considering plausible mechanisms through which this adduct may form. In light of our other observations, one obvious pathway involves oxidation of the dissociated ligand and binding of the resulting bipyridyl *N*-oxide to a Ru center. The fact that **8** is a Ru(II) complex (as indicated by MS) is, however, hard to rationalize given the excess amount of H_5IO_6 that is present under the reaction conditions. In addition, the low pH of the reaction medium would be expected to protonate dtbpy and therefore disfavor ligand *N*-oxidation.[36] Accordingly, further experiments were designed to query the mechanism of formation of **8** and the likelihood that this adduct is an arrested state of the catalyst.

To test if dtbpy *N*-oxide functions as a catalyst poison, varying quantities of this material were added to a hydroxylation reaction of **5** performed under standard conditions (Table 2). Remarkably, even small amounts of

Table 2. Catalyst Poisoning by dtbpy *N*-Oxide[a]

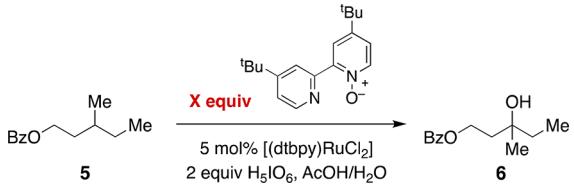

entry	*N*-oxide (equiv)	[*N*-oxide] (mM)	% Conversion	TON
1	0	0	58	11.6
2	0.001	0.0625	32	6.4
3	0.005	0.313	28	5.6
4	0.010	0.625	12	2.4
5	0.050	3.125	<5	<1.0

[a]Conditions: 5 mol % *cis*-[(dtbpy)$_2$RuCl$_2$] (3.125 mM), dtbpy *N*-oxide, 2.0 equiv of H_5IO_6 (125 mM), AcOH/H_2O, 1 h. Product conversions estimated by ^{1}H NMR integration of unpurified reaction mixtures against an internal standard.

the *N*-oxide (0.1 mol %) reduced product conversion by ~2-fold (entry 2). With 5 mol % of this additive, the reaction was completely shut down (entry 5). Subsequent experiments showed that the addition of free ligand, dtbpy, was similarly deleterious to catalyst performance.[37] In addition, only trace alcohol product **6** was obtained when the bpy-derived tris-complex was tested as a precatalyst (see Supporting Information for details). Together, these findings provide compelling evidence that formation of **8** is a principal pathway for catalyst deactivation in reactions with **1** (Figure 10). The two other bipyridyl complexes, **2** and **3**, are more susceptible to ligand dissociation, and thus this alternative channel for catalyst arrest may play a less prevalent role in affecting TONs.

At present, the mechanism of formation of the tris-(bipyridyl)Ru(II) complex **8** remains outstanding. Our finding that catalyst turnover is retarded by the addition of small quantities of free ligand (dtbpy) would seem to favor the pathway outlined above. It is possible, however, that *N*-oxide formation occurs through a unimolecular event in which the bound bipyridyl ligand is directly oxidized.[38]

CONCLUSIONS

Continuing efforts to develop Ru catalysts for chemoselective C(sp^3)−H oxidation have motivated the studies described herein. As with many redox processes, mechanistic analysis is challenged by the fleeting lifetime of intermediates, the presence of more than one chemically competent active species, and the multifarious pathways for catalyst decomposition and/or arrest. As an analytical method, the ability to monitor reaction progress using high mass-accuracy mass spectrometry is differential. For our purposes, by pairing PSI-MS with electrochemical and kinetic measurements, we have gained a comprehensive understanding of the chemistry of bis(bipyridyl)Ru complexes as oxidation catalysts. These insights include (1) support for Ru(VI) and Ru(V)-oxo complexes as active hydroxylating agents; (2) direct evidence of ligand dissociation; (3) affirmation that the rate of bipyridyl

DOI: 10.1021/jacs.8b10950
J. Am. Chem. Soc. 2019, 141, 972−980

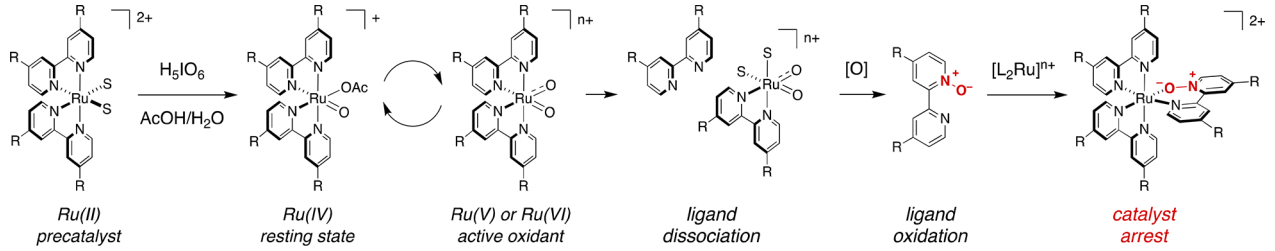

Figure 10. Proposed mechanisms of degradation of bis(bipyridyl)Ru catalysts under oxidative conditions.

exchange is influenced by 4,4′-substitution; and (4) characterization of three different pathways that limit catalyst TONs: dimerization, ligand loss, and catalyst poisoning by bipyridyl *N*-oxide formation. These findings are testament to the transformative power of PSI-MS for methods research and development, and have provided an unexpected level of clarity to the mechanistic complexities of our Ru-catalyzed C−H hydroxylation reaction.

■ ASSOCIATED CONTENT

Supporting Information

The Supporting Information is available free of charge on the ACS Publications website at DOI: 10.1021/jacs.8b10950.

Experimental details, characterization data, and PSI-MS analysis (PDF)

■ AUTHOR INFORMATION

Corresponding Authors

*rnz@stanford.edu
*sigman@chem.utah.edu
*waymouth@stanford.edu
*jdubois@stanford.edu

ORCID

James B. C. Mack: 0000-0001-7033-1014
Katherine L. Walker: 0000-0002-7924-8185
Richard N. Zare: 0000-0001-5266-4253
Matthew S. Sigman: 0000-0002-5746-8830
Robert M. Waymouth: 0000-0001-9862-9509
J. Du Bois: 0000-0001-7847-1548

Notes

The authors declare no competing financial interest.

■ ACKNOWLEDGMENTS

We thank the National Science Foundation under the Center for Chemical Innovation in Selective C−H Functionalization (CHE-1700982), the Air Force Office of Scientific Research Initiative (AFOSR FA9550-16-1-0113), and Novartis Pharmaceuticals for financial support of this work. J.B.C.M. and K.L.W. are grateful to the Center for Molecular Analysis and Design (CMAD, Stanford University) for research fellowships. K.L.W. and S.G.R. would like to thank the NSF for graduate research fellowships.

■ REFERENCES

(1) For recent reviews, see: (a) Godula, K.; Sames, D. C−H Bond Functionalization in Complex Organic Synthesis. *Science* **2006**, *312*, 67−72. (b) Newhouse, T.; Baran, P. S. If C−H Bonds Could Talk: Selective C−H Bond Oxidation. *Angew. Chem., Int. Ed.* **2011**, *50*, 3362−3374. (c) McMurray, L.; O'Hara, F.; Gaunt, M. J. Recent Developments in Natural Product Synthesis Using Metal-Catalysed C−H Bond Functionalisation. *Chem. Soc. Rev.* **2011**, *40*, 1885−1898. (d) Yamaguchi, J.; Yamaguchi, A. D.; Itami, K. C−H Bond Functionalization: Emerging Synthetic Tools for Natural Products and Pharmaceuticals. *Angew. Chem., Int. Ed.* **2012**, *51*, 8960−9009. (e) Tao, P.; Jia, Y. C−H Bond Activation in the Total Syntheses of Natural Products. *Sci. China: Chem.* **2016**, *59*, 1109−1125. (f) Domingo, V.; Quilez del Moral, J. F.; Barrero, A. F. Recent Accomplishments in the Total Synthesis of Natural Products Through C−H Functionalization Strategies. *Stud. Nat. Prod. Chem.* **2016**, *48*, 1−28. (g) Cernak, T.; Dykstra, K. D.; Tyagarajan, S.; Vachal, P.; Krska, S. W. The Medicinal Chemist's Toolbox for Late Stage Functionalization of Drug-like Molecules. *Chem. Soc. Rev.* **2016**, *45*, 546−576. (h) Ping, L.; Chung, D. S.; Bouffard, J.; Lee, S. Transition Metal-Catalyzed Site- and Regio-Divergent C−H Bond Functionalization. *Chem. Soc. Rev.* **2017**, *46*, 4299−4328. (i) Saint-Denis, T. G.; Zhu, R.-Y.; Chen, G.; Wu, Q.-F.; Yu, J.-Q. Enantioselective C(sp^3)−H Bond Activation by Chiral Transition Metal Catalysts. *Science* **2018**, *359*, No. eaao4798. (j) Karimov, R. R.; Hartwig, J. F. Transition-Metal-Catalyzed Selective Functionalization of C(sp^3)−H Bonds in Natural Products. *Angew. Chem., Int. Ed.* **2018**, *57*, 4234−4241.

(2) (a) Chorghade, M. S.; Hill, D. R.; Lee, E. C.; Pariza, R. J.; Dolphin, D. H.; Hino, F.; Zhang, L.-Y. Metalloporphyrins as Chemical Mimics of Cytochrome P-450 Systems. *Pure Appl. Chem.* **1996**, *68*, 753−756. (b) Sawayama, A. M.; Chen, M. M. Y.; Kulanthaivel, P.; Kuo, M.-S.; Hemmerle, H.; Arnold, F. H. A Panel of Cytochrome P450 BM3 Variants to Produce Drug Metabolites and Diversify Lead Compounds. *Chem. - Eur. J.* **2009**, *15*, 11723−11729. (c) Cusack, K. P.; Koolman, H. F.; Lange, U. E. W.; Peltier, H. M.; Piel, I.; Vasudevan, A. Emerging Technologies for Metabolite Generation and Structural Diversification. *Bioorg. Med. Chem. Lett.* **2013**, *23*, 5471−5483. (d) Genovino, J.; Sames, D.; Hamann, L. G.; Touré, B. B. Accessing Drug Metabolites via Transition-Metal Catalyzed C−H Oxidation: The Liver as Synthetic Inspiration. *Angew. Chem., Int. Ed.* **2016**, *55*, 14218−14238. (e) Blakemore, D. C.; Castro, L.; Churcher, I.; Rees, D. C.; Thomas, A. W.; Wilson, D. M.; Wood, A. Organic Synthesis Provides Opportunities to Transform Drug Discovery. *Nat. Chem.* **2018**, *10*, 383−394.

(3) (a) Genovino, J.; Lütz, S.; Sames, D.; Touré, B. B. Complementation of Biotransformations with Chemical C−H Oxidation: Copper-Catalyzed Oxidation of Tertiary Amines in Complex Pharmaceuticals. *J. Am. Chem. Soc.* **2013**, *135*, 12346−12352. (b) Rasik, C. M.; Brown, M. K. Total Synthesis of Gracilioether F: Development and Application of Lewis Acid Promoted Ketene-Alkene [2 + 2] Cycloadditions and Late-Stage C−H Oxidation. *Angew. Chem., Int. Ed.* **2014**, *53*, 14522−14526. Hung, K.; Condakes, M. L.; Morikawa, T.; Maimone, T. J. Oxidative Entry into the Illicium Sesquiterpenes: Enantiospecific Synthesis of (+)-Pseudoanisatin. *J. Am. Chem. Soc.* **2016**, *138*, 16616−16619. (c) Griffiths, R. J.; Burley, G. A.; Talbot, E. P. A. Transition-Metal-Free Amine Oxidation: A Chemoselective Strategy for the Late-Stage Formation of Lactams. *Org. Lett.* **2017**, *19*, 870−873. (d) Gan, P.; Pitzen, J.; Qu, P.; Snyder, S. A. Total Synthesis of the Caged Indole Alkaloid Arboridinine Enabled by Aza-Prins and Metal-Mediated Cyclizations. *J. Am. Chem. Soc.* **2018**, *140*, 919−925.

(4) For representative examples of C−H oxidation of natural products and active pharmaceutical ingredients, see: (a) McNeill, E.; Du Bois, J. Catalytic C−H Oxidation by a Triazamacrocyclic Ruthenium Complex. *Chem. Sci.* **2012**, *3*, 1810−1813. (b) Gormisky,

DOI: 10.1021/jacs.8b10950
J. Am. Chem. Soc. 2019, 141, 972−980

P. E.; White, M. C. Catalyst-Controlled Aliphatic C−H Oxidations with a Predictive Model for Site-Selectivity. *J. Am. Chem. Soc.* **2013**, *135*, 14052−14055. (c) Adams, A. M.; Du Bois, J. Organocatalytic C−H Hydroxylation with Oxone® Enabled by an Aqueous Fluoroalcohol Solvent System. *Chem. Sci.* **2014**, *5*, 656−659. (d) See, Y. Y.; Herrmann, A. T.; Aihara, Y.; Baran, P. S. Scalable C−H Oxidation with Copper: Synthesis of Polyoxypregnanes. *J. Am. Chem. Soc.* **2015**, *137*, 13776−13779.

(5) Asensio, G.; González-Núñez, M. E.; Bernardini, C. B.; Mello, R.; Adam, W. Regioselective Oxyfunctionalization of Unactivated Tertiary and Secondary C-H Bonds of Alkylamines by Methyl-(Trifluoromethyl)Dioxirane in Acid Medium. *J. Am. Chem. Soc.* **1993**, *115*, 7250−7253.

(6) (a) Dangel, B. D.; Johnson, J. A.; Sames, D. Selective Functionalization of Amino Acids in Water: A Synthetic Method via Catalytic C−H Bond Activation. *J. Am. Chem. Soc.* **2001**, *123*, 8149−8150. (b) Malik, H. A.; Taylor, B. L. H.; Kerrigan, J. R.; Grob, J. E.; Houk, K. N.; Du Bois, J.; Hamann, L. G.; Patterson, A. W. Non-Directed Allylic C−H Acetoxylation in the Presence of Lewis Basic Heterocycles. *Chem. Sci.* **2014**, *5*, 2352−2361. (c) Lee, M.; Sanford, M. S. Platinum-Catalyzed, Terminal-Selective C(sp^3)−H Oxidation of Aliphatic Amines. *J. Am. Chem. Soc.* **2015**, *137*, 12796−12799. (d) Howell, J. M.; Feng, K.; Clark, J. R.; Trzepkowski, L. J.; White, M. C. Remote Oxidation of Aliphatic C−H Bonds in Nitrogen-Containing Molecules. *J. Am. Chem. Soc.* **2015**, *137*, 14590−14593. (e) Adams, A. M.; Du Bois, J.; Malik, H. A. Comparative Study of the Limitations and Challenges in Atom-Transfer C−H Oxidations. *Org. Lett.* **2015**, *17*, 6066−6069. (f) Mbofana, C. T.; Chong, E.; Lawniczak, J.; Sanford, M. S. Iron-Catalyzed Oxyfunctionalization of Aliphatic Amines at Remote Benzylic C−H Sites. *Org. Lett.* **2016**, *18*, 4258−4261. (g) Lee, M.; Sanford, M. S. Remote C(sp^3)−H Oxygenation of Protonated Aliphatic Amines with Potassium Persulfate. *Org. Lett.* **2017**, *19*, 572−575. (h) Schultz, D. M.; Lévesque, F.; DiRocco, D. A.; Reibarkh, M.; Ji, Y.; Joyce, L. A.; Dropinski, J. F.; Sheng, H.; Sherry, B. D.; Davies, I. W. Oxy-functionalization of the Remote C−H Bonds of Aliphatic Amines by Decatungstate Photocatalysis. *Angew. Chem., Int. Ed.* **2017**, *56*, 15274−15278. (i) Olivo, G.; Farinelli, G.; Barbieri, A.; Lanzalunga, O.; Di Stefano, S.; Costas, M. Supramolecular Recognition Allows Remote, Site-Selective C−H Oxidation of Methylenic Sites in Linear Amines. *Angew. Chem., Int. Ed.* **2017**, *56*, 16347−16351. (j) Dantignana, V.; Milan, M.; Cussó, O.; Company, A.; Bietti, M.; Costas, M. Chemoselective Aliphatic C−H Bond Oxidation Enabled by Polarity Reversal. *ACS Cent. Sci.* **2017**, *3*, 1350−1358. (k) Nanjo, T.; De Lucca, E. C.; White, M. C. Remote, Late-Stage Oxidation of Aliphatic C−H Bonds in Amide-Containing Molecules. *J. Am. Chem. Soc.* **2017**, *139*, 14586−14591. (l) Jana, S.; Ghosh, M.; Ambule, M.; Sen Gupta, S. Iron Complex Catalyzed Selective C−H Bond Oxidation with Broad Substrate Scope. *Org. Lett.* **2017**, *19*, 746−749. (m) Kawamata, Y.; Yan, M.; Liu, Z.; Bao, D. H.; Chen, J.; Starr, J. T.; Baran, P. S. Scalable, Electrochemical Oxidation of Unactivated C−H Bonds. *J. Am. Chem. Soc.* **2017**, *139*, 7448−7451. (n) Cooper, J. C.; Luo, C.; Kameyama, R.; Van Humbeck, J. F. Combined Iron/Hydroxytriazole Dual Catalytic System for Site Selective Oxidation Adjacent to Azaheterocycles. *J. Am. Chem. Soc.* **2018**, *140*, 1243−1246.

(7) Mack, J. B. C.; Gipson, J. D.; Du Bois, J.; Sigman, M. S. Ruthenium-Catalyzed C−H Hydroxylation in Aqueous Acid Enables Selective Functionalization of Amine Derivatives. *J. Am. Chem. Soc.* **2017**, *139*, 9503−9506.

(8) Chan, S. L. F.; Kan, Y. H.; Yip, K. L.; Huang, J. S.; Che, C.-M. Ruthenium Complexes of 1,4,7-Trimethyl-1,4,7-Triazacyclononane for Atom and Group Transfer Reactions. *Coord. Chem. Rev.* **2011**, *255*, 899−919.

(9) Lee, S.; Fuchs, P. L. Chemospecific Chromium[VI] Catalyzed Oxidation of C−H Bonds at −40 °C. *J. Am. Chem. Soc.* **2002**, *124*, 13978−13979.

(10) Bipyridine complexes of Mn and Fe fail to catalyze hydroxylation when reactions are performed in aqueous acetic acid; see Supporting Information for details.

(11) *In situ* preparation of Ru complexes affords multiple products, as determined by ^{1}H NMR.

(12) Sullivan, B. P.; Salmon, D. J.; Meyer, T. J. Mixed Phosphine 2,2′-Bipyridine Complexes of Ruthenium. *Inorg. Chem.* **1978**, *17*, 3334−3341.

(13) Ashford, D. L.; Brennaman, M. K.; Brown, R. J.; Keinan, S.; Concepcion, J. J.; Papanikolas, J. M.; Templeton, J. L.; Meyer, T. J. Varying the Electronic Structure of Surface-Bound Ruthenium(II) Polypyridyl Complexes. *Inorg. Chem.* **2015**, *54*, 460−469.

(14) A Ru(II) precatalyst derived from 4,4′-bis(dimethylamino)-2,2′-bipyridine fails to catalyze C−H hydroxylation.

(15) Turnover differential between precatalysts is more pronounced at lower catalyst loadings.

(16) Cyclic voltammogram recordings were performed exclusively with Ru-carbonato complexes, as the corresponding dichloro adducts yielded featureless CVs.

(17) Dobson, J. C.; Meyer, T. J. Redox Properties and Ligand Loss Chemistry in Aqua/Hydroxo/Oxo Complexes Derived from *cis*- and *trans*-$[(bpy)_2Ru^{II}(OH_2)_2]^{2+}$. *Inorg. Chem.* **1988**, *27*, 3283−3291.

(18) (a) Che, C.-M.; Leung, W.-H. A *cis*-Dioxoruthenium(VI) Complex as Active Oxidant of Chloride and Organic Substrates; Preparation, Characterization, and Reactivity of *cis*-$[Ru^{VI}(6,6'\text{-}Cl_2bpy)_2O_2]^{2+}$. *J. Chem. Soc., Chem. Commun.* **1987**, *18*, 1376−1377. (b) Che, C. M.; Leung, W. H.; Li, C. K.; Poon, C. K. Synthesis, Reactivities and Electrochemistry of Trans-Dioxoruthenium(VI) Complexes of π-Aromatic Diimines. *J. Chem. Soc., Dalton Trans.* **1991**, *3*, 379−384. (c) Che, C.-M.; Cheng, K.-W.; Chan, M. C. W.; Lau, T.-C.; Mak, C.-K. Stoichiometric and Catalytic Oxidations of Alkanes and Alcohols Mediated by Highly Oxidizing Ruthenium−Oxo Complexes Bearing 6,6′-Dichloro-2,2′-Bipyridine. *J. Org. Chem.* **2000**, *65*, 7996−8000.

(19) Cyclic voltammograms of precatalyst **1** measured in either aqueous $HClO_4$ or a 1:1 mixture of $HClO_4$/AcOH showed similar redox behavior; see Figure S2 for comparison.

(20) (a) Che, C.-M.; Leung, W.-H.; Poon, C.-K. Oxidation of Organic Substrates Catalysed by *Trans*-$[Ru^{III}(phen)_2(OH)(OH_2)][ClO_4]_2$ and *Trans*-$[Ru^{III}(bpy)_2(OH)(OH_2)][ClO_4]_2$. *J. Chem. Soc., Chem. Commun.* **1987**, *3*, 173−175. (b) Lau, T. C.; Che, C. M.; Lee, W. O.; Poon, C. K. Ruthenium Catalysed Oxidation of Alkanes with Alkylhydroperoxides. *J. Chem. Soc., Chem. Commun.* **1988**, *21*, 1406−1407.

(21) We assume based on earlier work by Meyer (see ref 17) that Ru oxidants generated under chemical and electrochemical conditions are equivalent.

(22) Chiappini, N. D.; Mack, J. B. C.; Du Bois, J. Intermolecular C(sp^3)−H Amination of Complex Molecules. *Angew. Chem., Int. Ed.* **2018**, *57*, 4956−4959.

(23) (a) Vikse, K. L.; Ahmadi, Z.; Luo, J.; van der Wal, N.; Daze, K.; Taylor, N.; McIndoe, J. S. Pressurized sample infusion: An easily calibrated, low volume pumping system for ESI-MS analysis of reactions. *Int. J. Mass Spectrom.* **2012**, *323*−*324*, 8−13. (b) Yunker, L. P. E.; Stoddard, R. L.; McIndoe, J. S. Practical approaches to the ESI-MS analysis of catalytic reactions. *J. Mass Spectrom.* **2014**, *49*, 1−8. (c) Hesketh, A. V.; Nowicki, S.; Baxter, K.; Stoddard, R. L.; McIndoe, J. S. Simplified Real-Time Mass Spectrometric Analysis of Reactions. *Organometallics* **2015**, *34*, 3816−3819. (d) Theron, R.; Wu, Y.; Yunker, L. P. E.; Hesketh, A. V.; Pernik, I.; Weller, A. S.; McIndoe, J. S. Simultaneous Orthogonal Methods for the Real-Time Analysis of Catalytic Reactions. *ACS Catal.* **2016**, *6*, 6911−6917.

(24) Chromatographs of observed species are normalized by first dividing the maximum intensity Ru(102) peak in the isotope distribution by the total ion count at that time point. A second normalization factor is applied to set the maximum normalized intensity of each species in the ion chromatograph to "1".

(25) As noted previously, the carbonato and dichloro complexes perform identically for all substrates examined.

(26) Analogous trends were observed for precatalysts **2** and **3**, with signals corresponding to high-valent Ru compounds growing in sharply during the burst phase and decreasing rapidly as the reaction

DOI: 10.1021/jacs.8b10950
J. Am. Chem. Soc. 2019, 141, 972−980

ceases. Mass chromatograms and assignments of relevant ions for reactions with precatalysts **2** and **3** are available in the Supporting Information.

(27) For publications discussing a [3 + 2] mechanism of hydroxylation, see: (a) Bakke, J. M.; Lundquist, M.; Pedersen, U.; Rasmussen, P. B.; Lawesson, S.-O. The RuO_4 Oxidation of Cyclic Saturated Hydrocarbons. Formation of Alcohols. *Acta Chem. Scand.* **1986**, *40b*, 430−433. (b) Bakke, J. M.; Brænden, J. E.; Dahlin, B.-M.; Dahlman, O.; Enzell, C. R.; Pettersson, T. Derivatisation of Saturated Hydrocarbons. The Mechanism of RuO_4 Oxidations. *Acta Chem. Scand.* **1991**, *45*, 418−423. (c) Bakke, J. M.; Bethell, D.; Harrit, N.; Holm, A.; Spielbüchler, P.; Pedersen, J. B.; Krogsgaard-Larsen, P. The Mechanism of RuO_4-Mediated Oxidations of Saturated Hydrocarbons. Reactivity, Kinetic Isotope Effect and Activation Parameters. *Acta Chem. Scand.* **1992**, *46*, 644−649. (d) Bakke, J. M.; Frøhaug, A. E.; Kjekshus, A.; Springborg, J.; Wang, D.-N.; Paulsen, G. B.; Nielsen, R. I.; Olsen, C. E.; Pedersen, C.; Stidsen, C. E. The Mechanism of RuO_4-Mediated Oxidations of Saturated Hydrocarbons. Solvent Effects and Substituent Effects. *Acta Chem. Scand.* **1994**, *48*, 160−164. (e) Bakke, J. M.; Frøhaug, A. E. Ruthenium Tetraoxide Mediated Reactions: The Mechanisms of Oxidations of Hydrocarbons and Ethers. *J. Phys. Org. Chem.* **1996**, *9*, 310−318. (f) Bakke, J. M.; Frøhaug, A. E. Mechanism of RuO_4-Mediated Oxidations of Saturated Hydrocarbons, Isotope Effects, Solvent Effects and Substituent Effects. *J. Phys. Org. Chem.* **1996**, *9*, 507−513. (g) Drees, M.; Strassner, T. Ruthenium Tetraoxide Oxidations of Alkanes: DFT Calculations of Barrier Heights and Kinetic Isotope Effects. *J. Org. Chem.* **2006**, *71*, 1755−1760.

(28) For representative publications discussing stepwise C−H oxidation by oxo-metal species, see: (a) Groves, J. T.; McClusky, G. A. Aliphatic Hydroxylation via Oxygen Rebound. Oxygen Transfer Catalyzed by Iron. *J. Am. Chem. Soc.* **1976**, *98*, 859−861. (b) Filatov, M.; Harris, N.; Shaik, S. On the 'rebound' Mechanism of Alkane Hydroxylation by Cytochrome P450: Electronic Structure of the Intermediate and the Electron Transfer Character in the Rebound Step. *Angew. Chem., Int. Ed.* **1999**, *38*, 3510−3512.

(29) Ligand oxidation may represent a third pathway by which turnover is adversely effected. Such a process would yield a modified ligand that is presumably unable to support a high-valent Ru oxidant.

(30) Experiments with a mono(dtbpy)Ru precatalyst yielded only a single turnover, providing support to this claim; see Scheme S3 for details.

(31) (a) Collin, J. P.; Sauvage, J. P. Synthesis and Study of Mononuclear Ruthenium(II) Complexes of Sterically Hindering Diimine Chelates. Implications for the Catalytic Oxidation of Water to Molecular Oxygen. *Inorg. Chem.* **1986**, *25*, 135−141. (b) Cozzi, P. G. Metal-Salen Schiff Base Complexes in Catalysis: Practical Aspects. *Chem. Soc. Rev.* **2004**, *33*, 410−421. (c) Ingram, A. J.; Solis-Ibarra, D.; Zare, R. N.; Waymouth, R. M. Trinuclear Pd_3O_2 Intermediate in Aerobic Oxidation Catalysis. *Angew. Chem., Int. Ed.* **2014**, *53*, 5648−5652. (d) Flender, C.; Adams, A. M.; Roizen, J. L.; McNeill, E.; Du Bois, J.; Zare, R. N. Speciation and Decomposition Pathways of Ruthenium Catalysts Used for Selective C−H Hydroxylation. *Chem. Sci.* **2014**, *5*, 3309−3314.

(32) The lifetime of the mono(bpy)Ru complex is fleeting based on PSI-MS analysis, and thus it is unlikely that this intermediate functions as a competent oxidant.

(33) A mono-oxidized, tris-bipyridyl Ru complex has been characterized; see: Ghosh, P. K.; Brunschwig, B. S.; Chou, M.; Creutz, C.; Sutin, N. Thermal and Light-Induced Reduction of $Ru(bpy)_3^{3+}$ in Aqueous Solution. *J. Am. Chem. Soc.* **1984**, *106*, 4772−4783.

(34) Assignment of this structure is based on MS/MS analysis and comparison of chromatograms to those obtained from an authentic sample; see the Supporting Information for details.

(35) Analogous tris-Ru complexes were also detected in reactions with precatalysts **2** and **3**; see the Supporting Information for details.

(36) The dtbpy *N*-oxide complex **8** forms even if CF_3SO_2OH is added to the reaction mixture; see the Supporting Information for details.

(37) The effect of dtbpy *N*-oxide as a catalyst poison is less pronounced for reactions employing the dichloro adduct of **1**. An explanation for this result is not evident at this time.

(38) (a) Tatsumi, K.; Hoffmann, R. Metalloporphyrins with Unusual Geometries. 2. Slipped and Skewed Bimetallic Structures, Carbene and Oxo Complexes, and Insertions into Metal-Porphyrin Bonds. *Inorg. Chem.* **1981**, *20*, 3771−3784. (b) Mahy, J. P.; Battioni, P.; Mansuy, D. Formation of an Iron(III) Porphyrin Complex with a Nitrene Moiety Inserted into a Fe−N Bond during Alkene Aziridination by [(Tosylimido)Iodo]Benzene Catalyzed by Iron(III) Porphyrins. *J. Am. Chem. Soc.* **1986**, *108*, 1079−1080.

DOI: 10.1021/jacs.8b10950
J. Am. Chem. Soc. 2019, 141, 972−980